The dynamics of one-dimensional excitons in liquids

van Burgel, Mirjam; Wiersma, Douwe A.; Duppen, Koos

Published in:
Journal of Chemical Physics

DOI:
10.1063/1.469393

Publication date:
1995

The dynamics of one-dimensional excitons in liquids

Mirjam van Burgel, Douwe A. Wiersma, and Koos Duppen
Ultrafast Laser and Spectroscopy Laboratory, Department of Chemistry, Materials Science Center, University of Groningen, Nijenborgh 4, 9747 AG, Groningen, The Netherlands

(Received 1 August 1994; accepted 23 September 1994)

The properties of excitons in one-dimensional molecular aggregates, dissolved at room temperature in a liquid, were studied by means of femtosecond nonlinear optical experiments. Both the one-exciton band (i.e., Frenkel-excitons) and multiexciton bands contribute to the observed nonlinear optical response. The rapid motions in the liquid lead to ultrafast perturbations of the molecular energy levels. This localizes the excitons on limited sections of the chains of aggregated molecules. Ultrafast frequency-resolved pump–probe spectroscopy on the lowest two exciton bands was employed to determine the delocalization length of the optical excitations. The kinetics of the exciton populations was measured by ultrafast grating scattering experiments and time-resolved single photon counting. A model is described in which the multiexciton bands act as doorway states in the exciton–exciton annihilation process. These bands thereby determine the population decay of the Frenkel excitons at high excitation densities. Room temperature photon echo experiments show that stochastic perturbations of the exciton transition frequencies occur on two distinct time scales. In particular the slow components of the fluctuations are affected by motional narrowing, associated with the exciton delocalization length. It is therefore argued that the optical dephasing of excitons is directly related to the spatial extent of the excitation on the aggregate chain.

I. INTRODUCTION

Aggregates of molecules are nanostructures that have properties between those of a single molecule and bulk material. The size of these aggregates may be rather small (2–10 monomer units), such as for instance found for photosensitizing dye molecules on silver halogenides,[1] but they may also contain hundreds or thousands of molecules. Examples of such large aggregates are the light harvesting pigment molecules in natural photosynthetic antenna systems[2] and liquid solutions of certain kinds of dye molecules.[3] These systems have attracted a lot of attention, in particular in view of their optical properties, which are distinctly different from those of the single molecules that constitute the aggregate. A strong dependence on the size of the aggregate is observed, for instance of optical nonlinearities,[4,5] or of the superradiance decay rate.[6] Such enhancement arises due to excitonic interactions between the molecules, which cause delocalization of the optical excitation over the monomers of the aggregate.[7–9]

Whereas the intermolecular interaction is the driving force for delocalization of the excitation over the entire aggregate, energetic disorder in the single-molecule energies or in the couplings between the molecules tend to localize the excited-state wave function on a finite section of the aggregate.[10] The delocalization range is then determined by the relative magnitude of the intermolecular coupling compared to the energetic disorder, instead of by the physical size of the aggregate. The size dependence of the optical properties thus only exists for aggregates that are small compared to this delocalization (or coherence-) length. For larger aggregates the localization limits the expected enhancement of the optical response, although the exciton may propagate in an incoherent way over the entire physical size of the aggregate.

In the past decade, the effects of energetic disorder on the localization of excitation and the corresponding reduction of collective effects in the (non-) linear optical response was extensively studied.[11–18] This was usually done for static disorder, neglecting dynamic aspects due to coupling of the excitonic system with a heat bath. Then the description of localization can be done within a simple eigenstate picture; the Hamiltonian in the basis set of the single-molecule site-eigenfunctions, with off-diagonal elements due to intermolecular couplings, is diagonalized to yield the delocalized exciton energies in the basis set of exciton wave functions. The energetic disorder is taken into account by assuming a static distribution in single-molecule energies and/or intermolecular couplings. This picture in principle only holds for zero-temperature, since coupling with a heat bath is not explicitly considered in the transition from the single-molecule to the exciton picture.

At finite temperatures, the single-molecule energies and intermolecular couplings fluctuate in a random manner, leading to energetic disorder of a dynamical nature. Again, even in the absence of static disorder, localization of the excitation is expected. This is a more complicated process than the zero-temperature case, where the localization is fully determined by the balance between the intermolecular coupling and the energetic disorder. At room temperature, the time scales that are associated with the coherent motion of the exciton and with the solvent perturbations, have to be considered as well.

For aggregates in liquid solution, at room temperature, the dynamical aspects of the disorder cannot be ignored. The single-molecule energy levels are subject to very rapid perturbations from the solvent molecules. For individually solvated molecules this leads to ultrafast dephasing of the optical transitions, which was in recent years extensively studied

 0021-9606/95/102(1)/20/14/$6.00

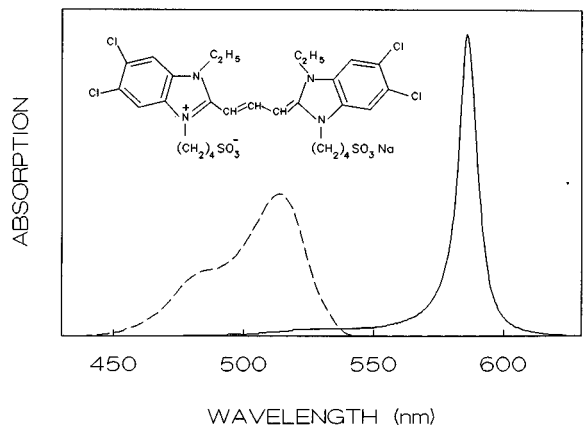

FIG. 1. Room temperature absorption spectra of TDBC in water. At very low concentration ($c \ll 10^{-6}$ M) absorption of monomers is observed (dashed line). At a concentration of $c = 5 \times 10^{-5}$ M, hardly any monomer absorption is visible anymore (solid line), since the molecules have aggregated into long one-dimensional chains. The red-shifted absorption at 587 nm is due to the excitation of Frenkel excitons on these chains. The molecular structure of TDBC is shown in the inset.

by a number of ultrafast techniques, such as transient hole burning,[19] two- and three-pulse photon echoes,[20–26] and chirped four-wave mixing.[27,28] For aggregates, the fluctuations lead to optical dephasing of the exciton optical transitions, and in addition they lead to localization of the excitation. Therefore, the spatial extent of the exciton and the optical dephasing of the exciton transitions are both determined by the same physical phenomenon: the coupling of the aggregate energy levels with a heat bath. A microscopic theory of this connection has not been formulated, yet.

The nature of the optical transitions of room temperature aggregates as well as their dynamics are presently not very well known. In this paper, the level structure and the dynamics of a linear aggregate, called TDBC, will be studied in liquid solution by ultrafast optical experiments. In Fig. 1, the absorption spectrum of TDBC-molecules in water is shown, together with the chemical structure of this molecule. The monomer absorption spectrum can only be observed at very low concentrations ($\ll 10^{-6}$ M). As the concentration is increased, a sharp band appears that is considerably red-shifted from the maximum of the monomer absorption band. This new feature is due to the aggregation of the TDBC molecules.

We report here on ultrafast pump–probe experiments on the exciton bands of these aggregates, which provides information on the spatial extent of the excitons. Grating scattering, time-resolved photon counting and photon echo experiments were employed to characterize the population decay and dephasing dynamics of the excitons under various excitation conditions. The results of all experiments are interpreted in terms of a single model, based on conventional exciton band theory for one-dimensional molecular systems, with stochastic fluctuations of the transition frequencies at two, ultrafast time scales.

The paper is organized as follows: In Sec. II, the various experiments and the sample handling will be described. In Sec. III, some aspects of the conventional theory for one-dimensional molecular excitons will be briefly reviewed. This part of the paper provides the background for the discussion of the experimental results, reported in the other sections of this paper. In Sec. IV, results of pump–probe experiments will be analyzed. In these nonlinear experiments, the presence of multiexciton bands clearly shows up. This feature can be used to determine the delocalization length of the excitons. In Sec. V, results of exciton lifetime experiments will be discussed. The relaxation time is shown to depend on excitation density, which points to contributions from higher exciton bands to the observed decay, or exciton–exciton annihilation of one-excitons as a decay channel. A simple kinetic picture of this process is presented, in which the multiexciton bands act as doorway states in the annihilation process. In Sec. VI, the optical dephasing of the exciton transitions is described, as measured in two-pulse photon echo experiments. When large pulse angles are used, coherences at the various multiexciton transitions give rise to intensity dependent phenomena. In the low pulse-angle limit, the dynamics of the optical transitions of the lowest two exciton-bands is measured. Motional averaging of the exciton over part of the solvent fluctuations is shown to occur. Finally, in Sec. VII, our findings are summarized and some conclusions are drawn regarding a full microscopic description that connects optical dephasing and localization of these excitonic systems.

II. EXPERIMENT

TDBC is the sodium salt of 1,1′-diethyl-3,3′-bis(4-sulfobutyl)-5,5′,6,6′-tetrachloro-benzimidazolo carbocyanine. This material was purchased from NKS (Japan Research Institute for Photosensitizing Dyes Co., Tokyo, Japan) and used by us without further purification. Aggregation occurred spontaneously when TDBC was dissolved in bidistilled water with a concentration of about 5×10^{-5} M. The pH of the solution was carefully adjusted at 11.0 by adding NaOH, to prevent dye protonation. No monomers were observed in any of the absorption spectra of the samples that were used for the time-resolved experiments. The sample consisted of a flowing jet stream with a thickness of about 200 μm. The optical density varied with concentration and thickness of the jet from O.D. 0.4 up to O.D. 0.8 for light polarized parallel to the direction of the flow. Due to the orientation of the linear aggregates in the jet stream, the optical density was about twice as low for polarization perpendicular to the direction of the flow.

The optical set-up, used for the photon echo, grating scattering, and pump–probe experiments, was the same as described previously.[29] Pulses from a colliding-pulse-modelocked (CPM) dye-laser (homebuilt), pumped by an argon ion laser (Coherent 90-6), were amplified by a copper-vapor laser (Oxford Lasers, ACL 35) at a repetition rate of 8.3 kHz. Part of the amplified light (pulse energy 10 nJ) was injected into an optical fiber to increase the spectral bandwidth by self-phase modulation. Subsequently, the light beam was sent through a compressor, consisting of a set of two gratings and four prisms. This yielded a pulse duration of 10 fs, as mea-

sured by an autocorrelation experiment in a 100 μm thick KDP crystal.

Depending on the requirements of the experiments, either two or three excitation and probe pulses were employed. At the sample, the energy of each 10 fs pulse was about 0.2 nJ ($\approx 6\times10^8$ photons/pulse). Focused with a 75 mm focal length lens, this gives a (two-level-) pulse angle of more than $\Theta=\pi/2$ on the strongest aggregate exciton transition (see Sec. VI). At times neutral-density filters were used to limit the pulse energy to the small-angle (perturbative-) limit. To maintain short pulse durations at the sample, the pulse compressor was then readjusted to precompensate for the optical dispersion in the filters.

The coherent signals were observed as a function of the delay between the excitation and probe pulses. In case of the photon echo and grating scattering experiments, the average power of the signal was detected by a photomultiplier (EMI 9816), and processed by a lock-in amplifier (EG&G 5209) operating at 1.2 kHz. In case of the pump–probe experiments, differential absorption spectra were obtained by taking the difference of the probe absorption spectrum with and without pumping pulses present. These spectra were recorded with an OMA-system (Princeton Instruments ST1000).

Time-correlated single photon counting was performed using a microchannel plate detector (Hamamatsu 1534-U01V), mounted on a simple prism monochromator. The fluorescence was induced with one of the femtosecond pulses, while another one triggered the time-to-amplitude converter (Ortec 457). The overall response time of this set-up was about 40 ps.

III. ONE-DIMENSIONAL MOLECULAR EXCITONS

When TDBC is dissolved in water at high concentration ($c>10^{-5}$ M), aggregates are formed which presumably have a linear, quasi-one-dimensional structure.[30,31] As shown in Fig. 1, a relatively sharp aggregate absorption band (FWHM 250 cm^{-1}) is observed at 587 nm, red-shifted from the maximum of the broad monomer absorption band at 513 nm (FWHM 900 cm^{-1}). This new feature is due to the intermolecular coupling between the TDBC molecules, which causes delocalization of the electronic excitations of TDBC over many sites of the aggregate. This is usually modeled in terms of linear chains of two-level systems with parallel transition dipoles of magnitude μ.[7–9,11–17] Without going into detail, we will briefly describe here how N coupled two-level systems give rise to 2^N aggregate levels, and how these separate into exciton bands in which a certain number of single-molecule excitations is present.

The electronic states of the aggregate can be described by the Frenkel-exciton Hamiltonian,[32]

$$\hat{\mathscr{H}}=\hbar\sum_{n=1}^{N}\omega_n(\hat{b}_n^{\dagger}\hat{b}_n)+\hbar\sum_{\substack{n,m=1\\ n\neq m}}^{N}V_{nm}(\hat{b}_n^{\dagger}\hat{b}_m+\hat{b}_m^{\dagger}\hat{b}_n)$$

$$\equiv\sum_{n,m=1}^{N}H_{nm}(\hat{b}_n^{\dagger}\hat{b}_m). \tag{1}$$

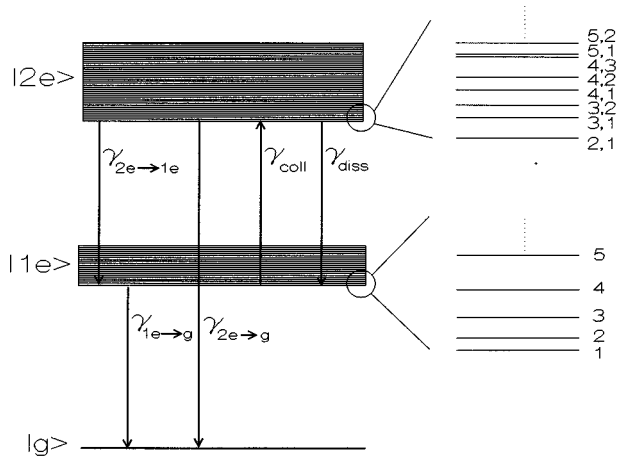

FIG. 2. Level structure of linear aggregates. There are N exciton bands, of which the lowest two are shown. The one-exciton band has a width of $2V$ and consists of N states, labeled by quantum number k. The two-exciton band has a width of $4V$ and contains $N(N-1)/2$ states, labeled by quantum numbers k_1 and k_2 ($k_1>k_2$). The states at the bottom of the band, that determine the optical response, are shown enlarged at the right with their corresponding quantum numbers. The scale of the enlargement is determined by the number of states in the band. The rate constants γ are discussed in Sec. V.

Here, ω_n is the transition frequency of molecule n, $\hat{b}_n^{\dagger}$ and $\hat{b}_n$ are the conventional Pauli creation and annihilation operators for an excitation on molecule n, and V_{nm} is the interaction between molecules n and m. When only nearest-neighbor coupling ($V_{nm}=V_{n,n\pm1}$) is considered, the Jordan–Wigner transformation converts the Paulions of Eq. (1) into noninteracting Fermions, which has the important advantage that all 2^N eigenstates of the aggregate can be obtained from the diagonalization of the $N\times N$ matrix $\hat{\mathscr{H}}_F$.[33–35] The Hamiltonian $\hat{\mathscr{H}}_F$ is identical to Eq. (1), but $\hat{b}_n^{\dagger}$ and $\hat{b}_n$ are now Fermion creation and annihilation operators.[33–35]

Since the number of excitations is conserved in the operation of $\hat{\mathscr{H}}_F$, the aggregate eigenstates separate into N different sets of linear combinations of single-molecule states, each with a fixed number of single-molecule excitations present. These are the one-, two-, three-, ..., N-exciton bands, of which the lowest two are displayed in Fig. 2. The ith band contains $\binom{N}{i}$ states, which are labeled with quantum numbers $k_1>k_2>\cdots>k_i$ with $k=1,...,N$. A general eigenstate in the ith band can be written as

$$|k_1,k_2,\ldots,k_i\rangle=\sum_{\substack{n_1,n_2\ldots n_i=1\\ n_i>\cdots n_2>n_1}}^{N}\det(\phi_{k_1n_1},\phi_{k_2n_2},\ldots,\phi_{k_in_i})\times|n_1,n_2,\ldots,n_i\rangle \tag{2}$$

with eigenfrequency

$$\Omega_{k_1k_2\cdots k_i}=\Omega_{k_1}+\Omega_{k_2}+\cdots+\Omega_{k_i}. \tag{3}$$

Here $|n_1,n_2,...,n_i\rangle$ denotes a state where molecules $n_1,n_2,...,n_i$ are excited and the others are in the ground state, $\det(\cdots)$ denotes the Slater determinant of the components ϕ_{kn} of the normalized eigenvectors of $\hat{\mathscr{H}}_F$, and Ω_k is an eigen-

frequency associated with quantum number k. The operator for dipole transitions between these eigenstates is

$$\hat{P}=\sum_{n=1}^{N}\mu_n(\hat{b}_n^{\dagger}+\hat{b}_n), \tag{4}$$

where μ_n is the dipole matrix element of the single molecules. Equation (4) shows that optical transitions are only allowed between two consecutive exciton manifolds.

For homogeneous aggregates, in which all sites have the same energy ($\omega_n\equiv\omega$) and all intermolecular couplings are equal ($V_{n,n\pm1}\equiv V$), the delocalized eigenstates Eq. (2), the eigenfrequencies Eq. (3), and the transition probabilities Eq. (4) can be found analytically.[33–35] Energetic disorder (static and/or dynamic) can be included in the model, by assuming some distribution or dynamic behavior of the single-molecule frequencies and the intermolecular couplings, but then the diagonalization of the Hamiltonian can only be performed numerically. For small disorder (compared to the intermolecular coupling), the homogeneous eigenstates form a good starting point for perturbative treatments.[12,13,17]

We will use the general results of homogeneous aggregates here as well, before we treat stochastic perturbations of the energy levels in Sec. VI. The fact that disorder leads to localization and optical dephasing is then taken care of in a phenomenological way. One immediate consequence is that the number of molecules N, which appears in Eqs. (1), (2), and (4), does not refer to the physical size of the aggregates anymore, due to the localization. The excitation only extends over an, as yet unknown, smaller subsection of the aggregate chain. This means that N now designates the delocalization length of the excitons, instead of the physical length.

For homogeneous aggregates, the components ϕ_{kn} of the eigenvectors are analytically derived to be[33–35]

$$\phi_{kn}=\sqrt{\frac{2}{N+1}}\sin\left(\frac{\pi kn}{N+1}\right) \tag{5}$$

and the eigenfrequencies Ω, associated with each quantum number k, are found to be

$$\Omega_k=\omega+2V\cos\left(\frac{\pi k}{N+1}\right). \tag{6}$$

By using these results in Eqs. (2)–(4), expressions for all 2^N eigenstates with the corresponding eigenvalues and transition moments can be found. We will briefly describe here some relevant aspects of the lowest exciton bands.

In the *one-exciton band*, N molecules on the aggregate chain share one single-molecule excitation. This band is centered at the single-molecule transition frequency ω, and has a width of four times the interaction energy V between the molecules in the chain. The delocalized states are the well-known Frenkel excitons,[32] which are characterized by a single quantum number k. The N eigenstates of this band follow from Eqs. (2) and (5),

$$|k\rangle=\sum_{n=1}^{N}\phi_{kn}|n\rangle=\sqrt{\frac{2}{N+1}}\sum_{n=1}^{N}\sin\left(\frac{\pi kn}{N+1}\right)|n\rangle \tag{7}$$

while the eigenfrequencies are given by Eq. (6). The states at the bottom of this band are shown enlarged on the lower right-hand side of Fig. 2. The transition moments from the ground state $|g\rangle$ to the various k-states of the one-exciton band are given by

$$\mu_{k,g}=\mu_{\mathrm{mon}}\sqrt{\frac{2}{N+1}}\frac{1-(-1)^k}{2}\cot\left[\frac{\pi k}{2(N+1)}\right]. \tag{8}$$

So, only states with an odd quantum number k have oscillator strength (dipole moment squared), and hence only these states are visible in a (linear-) absorption spectrum as displayed in Fig. 1. The state with $k=1$ contains by far the most oscillator strength: up to $0.81(N+1)\mu_{\mathrm{mon}}^2$ for $N\gg1$, which is about 81% of the total oscillator strength of the ground state to one-exciton transition. When the interaction energy V is negative (J-aggregates), which is the case for TDBC in water, this state can be found at the bottom of the one-exciton band [see Eq. (6)]. Hence, the aggregation leads to a red-shifted absorption compared to the monomer, with an asymmetric tail to the high-energy side where absorption occurs to the higher k states ($k=3,5,...$). The large oscillator strength of the $k=1$ state is responsible for exciton super-radiance at low temperatures.[6,13,15]

In the *two-exciton band*, N molecules on the aggregate chain share two single-molecule excitations. This band is centered at twice the single-molecule transition frequency ω, and has a width of eight times the interaction energy V between the molecules in the chain. Since optical transitions can only occur between two adjacent exciton bands, two-exciton states can only be probed by nonlinear optical experiments. Of course, this also hold for the higher exciton bands (the three-, four-,...,N-exciton bands). The states of the two-exciton band are characterized by two quantum numbers k_1 and k_2, which can take values from 1 to N ($k_1>k_2$). The eigenfrequencies are, according to Eq. (3), the sum of the two independent one-exciton eigenfrequencies associated with both k numbers. However, the wave functions of the two-exciton band are *not* the product of two independent one-exciton wave functions. This is a consequence of the Pauli exclusion principle; a molecule cannot be doubly excited. The $N(N-1)/2$ wave functions of the two-exciton band can be found by inserting Eq. (5) in Eq. (2),

$$\begin{aligned}|k_1,k_2\rangle&=\sum_{\substack{n_1,n_2=1\\ n_2>n_1}}^{N}(\phi_{k_1n_1}\phi_{k_2n_2}-\phi_{k_1n_2}\phi_{k_2n_1})|n_1,n_2\rangle\\ &=\frac{2}{N+1}\sum_{\substack{n_1,n_2=1\\ n_2>n_1}}^{N}\left[\sin\left(\frac{\pi k_1n_1}{N+1}\right)\sin\left(\frac{\pi k_2n_2}{N+1}\right)\right.\\ &\quad\left.-\sin\left(\frac{\pi k_1n_2}{N+1}\right)\sin\left(\frac{\pi k_2n_1}{N+1}\right)\right]|n_1,n_2\rangle.\end{aligned} \tag{9}$$

It immediately follows that states with the two quantum numbers k_1 and k_2 equal do not exist, due to the Pauli exclusion principle. Hence, the lowest energy state of the two-exciton band is *not* $k_1=1$, $k_2=1$, but $k_1=2$, $k_2=1$. Conse-

quently, the energy difference between the bottom of the one- and two-exciton bands is larger than the energy difference between the ground state and the one-exciton band. This feature can be employed to determine the delocalization length of the exciton, as will be discussed in Sec. IV. The states at the bottom of the two-exciton band are shown enlarged on the upper right-hand side of Fig. 2.

The general expression for the transition moments between the k-states of the one-exciton band and the k_1k_2-states of the two-exciton band, is given by[35]

$$\mu_{k_1k_2,k}=\mu_{\mathrm{mon}}\sqrt{\frac{2}{N+1}}\Bigg(\delta_{k_2,k}\frac{1+(-1)^{k_1}}{2}\cot\left[\frac{\pi k_1}{2(N+1)}\right]-\delta_{k_1,k}\frac{1+(-1)^{k_2}}{2}\cot\left[\frac{\pi k_2}{2(N+1)}\right]+1/2(\delta_{k_1-k_2-k,0}-\delta_{k_1-k_2+k,0})$$
$$\times\left\{\cot\left[\frac{\pi k_1}{2(N+1)}\right]+\cot\left[\frac{\pi k_2}{2(N+1)}\right]\right\}+1/2[\delta_{k_1+k_2+k,2(N+1)}-\delta_{k_1+k_2-k,0}]\left\{\cot\left[\frac{\pi k_1}{2(N+1)}\right]-\cot\left[\frac{\pi k_2}{2(N+1)}\right]\right\}\Bigg). \qquad (10)$$

The properties of these transition moments are similar to those of the ground state to one-exciton band transitions. For instance, the dominant transition from the one-exciton $k=1$ state is toward the $k_1=2$, $k_2=1$ state of the two-exciton manifold, which is located at the bottom of that band. The oscillator strength of this transition is $1.27(N+1)\mu_{\mathrm{mon}}^2$ for $N\gg1$, which is about 70% of the total oscillator strength of the $k=1$ one-exciton state to the two-exciton band.

Expressions for states in the higher exciton bands can be obtained in the same way, using Eqs. (2)–(6). These we will not write down explicitly here. Before we finish this section on the theoretical background, we will briefly summarize the most important simplifying assumptions that were introduced, to be able to assess the validity of the theory for the interpretation of the experimental results of the following sections.

Since we employ the results of homogeneous aggregate theory as a basis for a treatment of localization effects and optical dynamics, the quantum numbers $k_1,...,k_i$ have to be relevant for the identification of quantum states in the presence of static or dynamic disorder. The various states in an exciton band can in principle be identified when the linewidths of the transitions between these states are less than their energy separations $\Omega_k-\Omega_{k\pm1}$. Since the linewidth is determined by damping processes, and the separation by the delocalization length N, which itself is dependent on damping processes, this condition may always be fulfilled.

The theory holds for one-dimensional aggregates with only nearest-neighbor coupling. Fidder *et al.* showed that the exciton energy levels shift downward when interactions between all molecules are taken into account, instead of only nearest-neighbor couplings.[15] Additional shifts may also occur due to a difference in solvation energy of the aggregates compared to the monomer.[36] For the purpose of this paper on localization and optical dynamics of excitons in molecular aggregates, these effects are of minor importance. They mainly lead to a modification in the experimentally determined value of the nearest-neighbor coupling constant V,[37] and to a lesser extent of the delocalization length N.

A more important point is the neglect of exciton–exciton interactions in the calculations of the multiexciton bands. Such interactions may lead to states with a different character, for example biexcitons may be formed which are split-off from the two-exciton band.[38] In case of Frenkel excitons, the interactions are expected to be rather weak. It is at the moment not clear whether biexcitonic states play any role at all in the nonlinear optical response of molecular systems. Since so far no clear spectroscopic evidence has been reported for the existence of Frenkel interexcitonic interactions, we will neglect them in the remainder of this paper.

IV. EXCITON DELOCALIZATION LENGTH

The (non-) linear optical properties of aggregates depend on the delocalization length of the electronically excited states. In general, this length is not known, and models are required to extract it from the optical response. Localization of excitation is related to the breaking of translation symmetry, which in liquids has a dynamical nature. Consequently, depending on the time scale of the experiment, a distribution of exciton delocalization lengths will be found for an ensemble of excited aggregates. To determine the average number of TDBC molecules with coherently coupled electronic excited states, we investigated the level structure of the lowest two exciton bands. This was performed by pump–probe experiments with ultrashort light pulses.

In a pump–probe experiment on aggregate excitons, the pump pulse creates predominantly one-excitons in the lower k-states [see Eq. (8)]. These transitions are therefore bleached for the duration of the population lifetime of the excitons, which can be measured with a delayed probe pulse. In addition, the excited state population of one-excitons gives rise to absorption on the one- to two-exciton transitions. This was only recently demonstrated by Fidder *et al.*[39] and by Minoshima *et al.*[40] for PIC aggregates, and by Johnson *et al.*[41] for BIC aggregates. The absorption is somewhat blue-shifted compared to the bleach, which, as we will demonstrate, can be employed to determine the delocalization length of the excitons.

The strongest bleach on the transition from the ground state to the one-exciton band involves the $k=1$ state, with a transition frequency $\omega_{g\rightarrow k=1}=\omega+2V\cos[\pi/(N+1)]$, according to Eqs. (3) and (6). Here, ω is the single-molecule transition frequency of TDBC, and V is the intermolecular coupling in the TDBC-aggregate, as derived from the difference between the single-molecule (513 nm) and aggregate (587 nm) absorption maxima [Eq. (6) in the limit $N\gg1$ gives

$2V=2455\ \mathrm{cm}^{-1}$]. The strongest absorption from the $k=1$ one-exciton state involves the $k_1k_2=2,1$ state of the two-exciton band, as discussed in the previous section [Eq. (10)]. The frequency of this transition is, according to Eqs. (3) and (6), $\omega_{k=1\rightarrow k1k2=2,1}=\omega+2V\cos[2\pi/(N+1)]$. The difference between the pump-pulse induced bleach on the dominant ground state transition and the pump-pulse induced absorption on the dominant excited transition therefore is

$$\omega_{\mathrm{bleach}}-\omega_{\mathrm{absorption}}=2V\left[\cos\left(\frac{\pi}{N+1}\right)-\cos\left(\frac{2\pi}{N+1}\right)\right]\approx\frac{3\pi^2V}{(N+1)^2}, \tag{11}$$

where the approximate equality holds for $N\gg1$. This difference can be measured in a pump–probe experiment.

Equation (11) shows that the difference between bleach and induced absorption is a function of the delocalization length N. The reason for this dependence is the reduced phase space in the higher exciton bands. In the single-molecule picture this arises due to the fact that a two-level molecule cannot be excited twice. This was discussed in the previous section. For small delocalization lengths, the ''probability'' for two single-molecule excitations in the two-exciton band to be at the same site is higher than for large delocalization lengths. The difference between the various transitions therefore depends explicitly on the delocalization length.

In Figs. 3, results are shown of pump–probe experiments with short (10 fs) optical pulses. The differential spectrum is plotted, i.e., the difference in the probe absorption spectrum with and without the pump pulse. For a detailed analysis of these spectra, it does not suffice to look at only the two strongest transitions. More spectral components, although weaker, contribute to the observed line shapes. In addition, all lines are appreciably broadened by optical dephasing, so that the bleach and induced absorption partially overlap, which causes an artificial shift of the maxima. We therefore have to take into account the level structure of the exciton bands [Eqs. (2) and (5)], and the relevant transition moments [Eqs. (8) and (10)].

The 10 fs pump–pulse causes bleaching over the entire absorption spectrum of the aggregate, due to its large bandwidth. This means that the number of one-excitons, that are created in each k-state, is simply proportional to the oscillator strength $\mu_{k,g}^2$, given by Eq. (8), while the ground state population is reduced with a factor proportional to $\Sigma_k\mu_{k,g}^2$. The interaction of the probe pulse with the sample can be separated into three parts; (1) stimulated emission from the excited one-exciton k-states to the ground state ($\sim\mu_{k,g}^2$); (2) bleach of the absorption from the ground state to the one-exciton k'-states ($\sim\mu_{k',g}^2$), where k' is not necessarily equal to k; (3) induced absorption from the one-exciton k states to the two-exciton k_1k_2 states ($\sim\mu_{k1k2,k}^2$).

When we sum up all these contributions to the probe transmission, and subtract the probe absorption spectrum without the pump pulse present, the result is the differential absorption spectrum for zero pump–probe delay,

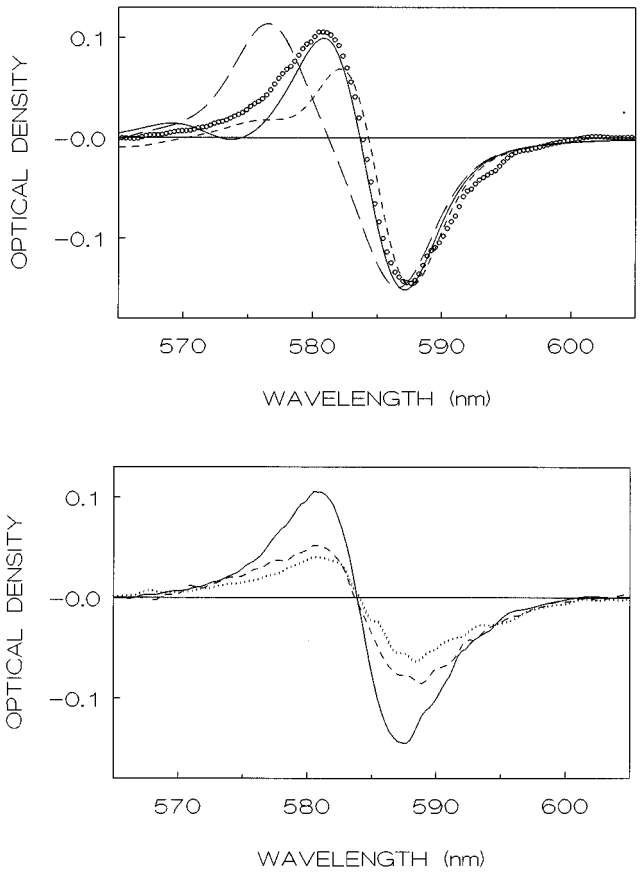

FIG. 3. (a) Frequency-resolved pump–probe signal of TDBC in water, performed with broad bandwidth optical pulses with a duration of 10 fs (open circles). The pump–probe delay is 0 fs. A bleach (negative signal) and an induced absorption (positive signal) partially overlap. The solid line is a simulation of the signal, based on Eq. (12) with a delocalization length of 15 TDBC-monomers. For comparison, the calculated results with exciton delocalization lengths of 10 monomers (long dashed) and 20 monomers (short dashed) are also shown. (b) Frequency-resolved pump–probe signal of TDBC in water for three different delays of the probe pulse; 0 fs (solid line), 200 fs (dashed line), and 2000 fs (dotted line). The rapid decrease of the signal at small delay is due to the coherent artefact that contributes to the signal when pump- and probe-pulses overlap in time.

$$\Delta A(\omega)=-\left[\sum_{k,k'}\mu_{k,g}^2\mu_{k',g}^2(1+\delta_{kk'})F(\omega_{g\rightarrow k}-\omega)\right]+\left[\sum_{k_1k_2,k}\mu_{k,g}^2\mu_{k_1k_2,k}^2F(\omega_{k\rightarrow k_1k_2}-\omega)\right]. \tag{12}$$

Here, it is assumed that the lineshape function $F(\omega)$ is the same for all transitions. It will be shown in Sec. VI, where the results of photon echo experiments are discussed, that this line shape function is determined by stochastic fluctuations of the transition frequencies at two different time scales. The form of $F(\omega)$ is given in Eq. (23).

Using Eq. (12), the initial pump–probe spectrum, before population relaxation becomes important, can be calculated. For the bleach signal, given by the first part of Eq. (12), all transitions between the ground state and the one-exciton band with k and/or $k'=1$, 3, 5, and 7 were taken into account. The transition moments $\mu_{k,g}$ are given by Eq. (8) and the transition frequencies $\omega_{g\rightarrow k}=\Omega_k$ by Eq. (6). Other states

in the one-exciton band were not considered, since the relevant oscillator strengths are negligible (less than 1% of the strongest transition). For the excited-state absorption signal (which has opposite sign compared to the bleach peak), the transitions from the one-exciton states $k=1$, 3, and 5 were considered. The largest transition moments $\mu_{k1k2,k}$ involve, according to Eq. (10), the two-exciton k_1k_2-states 21 and 32, 41 and 32, and 61 and 52, respectively. The transition frequencies $\omega_{k\rightarrow k1k2}=\Omega_{k1k2}-\Omega_k$ were calculated with Eqs. (3) and (6). It follows that a number of these transition are degenerate ($\omega_{1\rightarrow 21}=\omega_{3\rightarrow 32}=\omega_{5\rightarrow 52}$).

The calculated differential absorption spectrum is compared with the experiment in Fig. 3(a) for different delocalization lengths N. From the similarity between the calculation for $N=15$ and the experimental result, we can conclude that the average delocalization length of excitons of TDBC-aggregates in room temperature water is about 15 molecules. For lower values of N the maxima of the bleach and stimulated absorption are too far apart, while for higher values of N the bleach is too large compared to the stimulated absorption. The high energy side of the spectrum, where the calculated result for $N=15$ deviates substantially from the experimental result, may be affected by transitions from the two-exciton band to the three-exciton band and higher.[41,42]

In Fig. 3(b) is shown how the pump–probe signal rapidly decreases when very small delays are introduced between the pump- and probe-pulses, while for larger delays hardly any change seems to occur at all. The fast decrease of the signal does not represent ultrafast dynamics, such as has been suggested by Minoshima *et al.*[40] for PIC-aggregates at low temperature and Gagel *et al.*[43] for PIC aggregates at room temperature, since the decrease follows the pulse envelope. Instead, the additional signal around zero-delay is due to coherent coupling between both optical beams. This gives rise to the experimentally observed ''coherent artefact,'' that is well-known in pump–probe experiments on two-level systems. For three- or more-level systems such as aggregates a similar effect takes place; when the optical pulses overlap in time more permutations in field orderings contribute to the observed signal than at finite delay. Hence, a rapid initial decrease of the signal is observed for small delays.

For well-separated optical pulses, the development of the signal as a function of pump–probe delay does reflect the true dynamics of the system. We found that the decay of the pump–probe signal varied with excitation conditions. As we will show in Sec. V, this is probably due to intensity dependent (de-) population via higher exciton bands.

V. EXCITON POPULATION RELAXATION

For many aggregates, several population relaxation times have been reported. TDBC is no exception to this rule; Makio *et al.* reported an exciton lifetime of 62 ps,[30] while Lindrum *et al.* concluded that this lifetime was 96 ps.[31] It is now well-established that the experimental excitation intensity strongly influences the observed decay rate.[44–46] This is usually interpreted phenomenologically in terms of exciton–exciton annihilation,[46] without further specification of the physics of the annihilation process. Also, multiexponential decay is often observed,[31,40,43] which can in principle be explained in terms of a distribution of exciton delocalization lengths in the sample.[13] However, the decay times of the multiexponent may differ considerably,[31,40,43] which suggests that fundamentally different states contribute to the observed decay. We present here results on the population decay of TDBC in water, and interpret these in a simple kinetic model, based on population dynamics among the various exciton bands. Both the annihilation picture and multiexponential population decay can be obtained from this model when the proper limits of the decay parameters are taken.

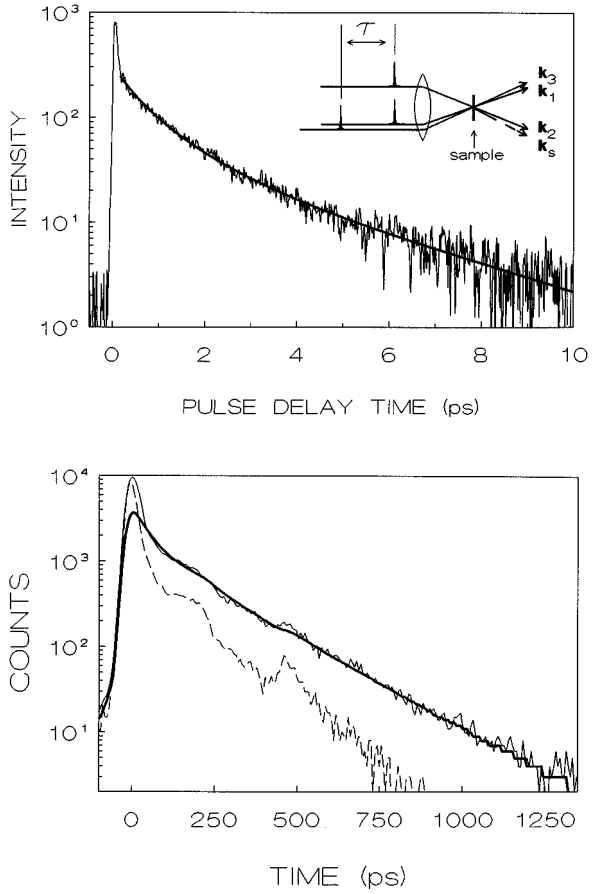

FIG. 4. (a) Grating scattering signal of TDBC in water, measured with 10 fs optical pulses. The layout of the experiment is shown in the inset. The probe beam $\mathbf{k}_3$ is not in the same plane as the excitation beams $\mathbf{k}_1$ and $\mathbf{k}_2$. The smooth solid curve is a calculation, based on the exciton–exciton annihilation model of Eq. (15) with parameters mentioned in the text. The grating scattering signal is proportional to $n_{1e}(t)$ squared. (b) Time-resolved single-photon counting decay of TDBC in water. The solid curve is the experiment and the dashed one the time response of the system, as measured from a nonabsorbing scattering medium. The smooth solid curve is a convolution of the system response with the exciton–exciton annihilation theory of Eq. (15). The photon counting signal is proportional to $n_{1e}(t)$.

In Fig. 4(a) the result is shown of a population-grating scattering experiment. Here, two femtosecond excitation pulses, with wave vectors $\mathbf{k}_1$ and $\mathbf{k}_2$, are crossed with an angle of $\sim 5°$ in the sample, in order to induce a spatially modulated distribution of excited aggregates. A third pulse, with wave vector $\mathbf{k}_3$, scatters from the resulting amplitude hologram in the phase-matched direction $\mathbf{k}_s=\mathbf{k}_3\pm(\mathbf{k}_2-\mathbf{k}_1)$. The beam geometry is shown in the inset of Fig. 4(a). When the delay of the third pulse is varied, the scattered intensity

reflects the dynamics of all exciton states that are involved in the formation of the population grating.[47,48]

The result of Fig. 4(a) shows a maximum in the signal when the third pulse overlaps in time with the excitation pulses. This effect is partly due to coherent coupling of all beams, similar to the coherent artefact of the pump–probe experiment discussed in Sec. IV. When the third pulse is well-separated in time from the excitation beams, a fast decay of the scattering signal of about 1.4 ps is observed. The interpretation seems to be clear; the population life time of the one-excitons is 2.8 ps (the factor of 2 is due to the fact that the signal is proportional to the spatially modulated population squared). However, the fact that the trace deviates significantly from being monoexponential indicates that this interpretation is not sufficient for a full description of the population decay process.

In Fig. 4(b) the result is shown of a fluorescence life time experiment, in which one femtosecond pulse is used to excite the sample and the emitted photons are individually timed at the detector. In this way the population dynamics of the excitons is studied as well, but now on a much longer time scale. The measured response contains a long component, which decays with a (close to monoexponential) time constant of 220 ps, and a short one that cannot be time-resolved by our setup, but that could very well be the 2.8 ps derived from the grating scattering experiment. The long component only makes up about 1% of the overall decay. Both components are emitted in the spectral range of the aggregate transitions; monomer emission or pump–pulse straylight do not contribute to these signals.

To connect the results of the grating scattering experiment with that of the single-photon counting experiment, we consider a simple kinetic model for the population dynamics in the one- and two-exciton bands. The level structure in each band is neglected (the emission is dominated by the strongest transition in each band), and higher multiexciton bands are not considered either. Extensions of the model which include these bands and the level structure are easily constructed. Here we concentrate on the essential features. The simplified population kinetics can thus be expressed in terms of the following differential equations:

$$\begin{aligned}
\frac{dn_g}{dt} &= +\gamma_{1e\to g} n_{1e} + \gamma_{2e\to g} n_{2e}, \\
\frac{dn_{1e}}{dt} &= -\gamma_{1e\to g} n_{1e} - \gamma_{\mathrm{coll}} n_{1e}^2 + (\gamma_{2e\to 1e} + 2\gamma_{\mathrm{diss}}) n_{2e}, \\
\frac{dn_{2e}}{dt} &= +\frac{\gamma_{\mathrm{coll}}}{2} n_{1e}^2 - (\gamma_{2e\to 1e} + \gamma_{2e\to g} + \gamma_{\mathrm{diss}}) n_{2e}.
\end{aligned} \tag{13}$$

Here, n_g, n_{1e}, and n_{2e} are the populations of the ground state and one- and two-exciton bands, respectively. The rates $\gamma_{1e\to g}$, $\gamma_{2e\to 1e}$, and $\gamma_{2e\to g}$ hold for the spontaneous relaxation processes of the exciton bands, in which photons are emitted or energy is released as heat to the material. The rate γ_{coll} describes a process in which the higher exciton band is populated from the lower one. In this picture, two excitations on the same aggregate chain, that are separated by more than the exciton delocalization length, are thought of as two independent one-excitons. These excitons propagate in a diffusive way along the chain, with a velocity that is probably to a large extent determined by the fluctuations of the molecular energy levels. A ''collision'' between two propagating one-excitons may then occur with a probability proportional to the one-exciton density squared. When this happens, two one-excitons are converted into one two-exciton. The inverse process is also taken into account, in which one two-exciton is converted into two one-excitons that are separated by more than the delocalization length. The rate constant for this ''dissociation'' process is γ_{diss}, which is also expected to be governed (in an as yet unknown way) by the energy fluctuations in the aggregate chain. All rate constants of Eq. (13) are depicted in Fig. 2.

Two limiting cases of Eqs. (13) give analytical solutions that were used previously in the analysis of nonexponential decay profiles of population relaxation in aggregates.[31,43–46] When it is assumed that the spatial diffusion of excitation is very slow, the rate constants γ_{coll} and γ_{diss} approach zero and the corresponding terms in Eqs. (13) can be neglected. The solution of Eqs. (13) for the excited state populations n_{1e} and n_{2e} of the one- and two-exciton bands then is

$$\begin{aligned}
n_{1e}(t) &= n_{1e}(0)\,\exp(-\gamma_{1e\to g} t) \\
&\quad + \frac{\gamma_{2e\to 1e} n_{2e}(0)}{\gamma_{2e\to 1e} + \gamma_{2e\to g} - \gamma_{1e\to g}} \{\exp(-\gamma_{1e\to g} t) \\
&\quad - \exp[-(\gamma_{2e\to 1e} + \gamma_{2e\to g}) t]\} \\
n_{2e}(t) &= n_{2e}(0)\,\exp[-(\gamma_{2e\to 1e} + \gamma_{2e\to g}) t].
\end{aligned} \tag{14}$$

Hence, if the population dynamics of both bands is measured simultaneously, biexponential behavior is observed, with the relative magnitude of both components determined by the excitation efficiency and emission cross section of both bands. Intensity dependence of the decay is thus expected. When more bands are included in the model, this result generalizes to multiexponential decays.

Our results from the grating scattering experiment and the single photon counting can thus be interpreted in the following way: the excitation pulse(s) populate both the one- and two-exciton bands. These relax according to Eqs. (14) with a total decay constant $(\gamma_{2e\to 1e}+\gamma_{2e\to g})^{-1}=2.8$ ps for the two-exciton band, and a decay constant $(\gamma_{1e\to g})^{-1}=220$ ps for the one-exciton band. However, the experimentally observed ratio of the two contributions (99% of the single photon counting decay occurs in 2.8 ps) can only be explained when the quantum yield for emission from the one-exciton band is much lower than for emission from the two-exciton band. This seems not very likely.

Another limit, in which Eqs. (13) can be solved analytically, is obtained when the lifetime of the two-exciton band is assumed to be very short, and dominated by the relaxation rate $\gamma_{2e\to 1e}$. At high excitation density, the population decay of the one-exciton band is then determined by collisional population of the two-exciton band, which subsequently rapidly relaxes back to the one-exciton band. In this process one of the two original colliding one-excitons is ''annihilated.'' The differential equation for the one-exciton population of

Eq. (13) then simplifies to $dn_{1e}/dt = -\gamma_{1e\to g} n_{1e} - \frac{1}{2}\gamma_{\mathrm{coll}} n_{1e}^2$, a form that was extensively used in the interpretation of fluorescence decays of PIC aggregates.[46] In this limit ($\gamma_{2e\to 1e} \to \infty$), the solution of Eqs. (13) for the excited state populations n_{1e} and n_{2e} of the one- and two-exciton bands is

$$n_{1e}(t) = \frac{2\gamma_{1e\to g} n_{1e}(0)\ \exp(-\gamma_{1e\to g} t)}{2\gamma_{1e\to g} + \gamma_{\mathrm{coll}} n_{1e}(0)[1-\exp(-\gamma_{1e\to g} t)]}, \qquad n_{2e}(t) \approx 0. \tag{15}$$

In this model intensity dependent population relaxation is expected as well, since the annihilation process depends on the population density of one-excitons squared.

Our results from the grating scattering experiment and the single photon counting can now be interpreted in a different way; the optical pulse(s) cause multiple excitations on each aggregate. Due to the limited exciton delocalization length of about 15 monomers, these excitations can be considered as independent one-excitons. The two-exciton band is also populated (two single-molecule excitations within the delocalization length), but relaxation from this band is extremely fast due, for instance, to coupling with highly excited single-molecule states or the conduction band of the aggregates. Therefore, population in this band is negligible and does not contribute to either the grating scattering signals or the single-photon counting decay [except perhaps around zero-delay, where it contributes to the observed additional peaks in Figs. 4(a) and 4(b)]. Since the one-excitons propagate in a diffusive manner, they may meet each other with a probability equal to the population density squared. Rapid depopulation then follows via excitation and decay of the two-exciton band. At long times, when the concentration of one-excitons has become so low that the collision probability vanishes, Eq. (15) predicts single-exponential decay; $n_{1e}(t) \sim \exp(-\gamma_{1e\to g} t)$.

The solid curves in Figs. 4(a) and 4(b) are calculated with the annihilation model of Eq. (15). To obtain the decay parameters from the fits, the initial excitation density must be known. This can be calculated from the optical density of the sample and the beam parameters of the optical pulses, when it is assumed that for every absorbed photon a one-exciton arises. This is most accurately done for the grating scattering experiment, because there the excitation is performed in focus. The relevant density of excitons was found to be $n_{1e}(0) = 1.55\times 10^{15}$ excitations $\mathrm{cm}^{-3}\,\mathrm{pulse}^{-1}$ for the experiment of Fig. 4(a). The decay constants are then derived to be $(\gamma_{1e\to g})^{-1} = 220$ ps for the spontaneous decay of the one-excitons, and $\gamma_{\mathrm{coll}} = 1.02\times 10^{-3}\ \mathrm{cm}^3\,\mathrm{s}^{-1}$ for the annihilation process. This last number is about a factor of 2 smaller than the annihilation values reported for PIC aggregates by Gagel *et al.*[43] and Sundström *et al.*[46] With our parameters one can calculate that the excitation intensity of the grating experiment should be a factor of 10^4 less than the intensities used here, in order to do experiments free from annihilation. With our detection sensitivity this limit could not be reached.

In Fig. 5 is shown how the decay of one-excitons occurs at a certain density. When the physical size of the TDBC aggregates is known, this curve could be used to calculate the mobility of the one-excitons. Currently, this size is unknown. In fact, it is at the moment not clear whether the annihilation limit of Eqs. (13) truly holds for TDBC. To determine this, it is necessary to perform additional population relaxation experiments as a function of excitation density, and in particular as a function of detection frequency, to assess the relative contributions to the signals from the various exciton bands. Such experiments are planned. For the moment it can be stated that the annihilation picture describes all population relaxation features well, with the exception of the strong grating scattering and photon counting signals around zero-delay. As stated above, coherent coupling between the optical beams will certainly contribute to the grating scattering signal when all pulses overlap in time, and resonance Rayleigh scattering may contribute to the fluorescence decay data at zero delay. However, it can at the moment not be excluded that incoherent population relaxation from the higher exciton bands contributes to these signals as well.

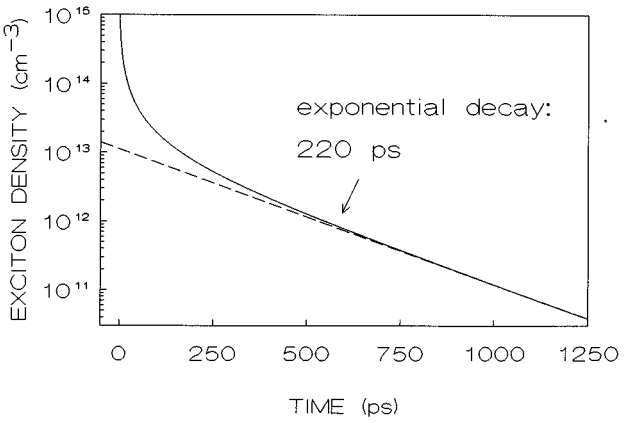

FIG. 5. Decay characteristics of one excitons in the annihilation model of Eq. (15). The sensitivity of our grating scattering setup is insufficient to detect a signal from exciton densities low enough to make annihilation negligible ($n_{1e} < 10^{-13}\ \mathrm{cm}^{-3}$).

VI. EXCITON DEPHASING DYNAMICS

The optical absorption spectrum of TDBC in water (Fig. 1) does not show a well-defined sequence of lines, corresponding to excitation of the various k-states depicted in Fig. 2. Considerable line broadening is present due to coupling between the excitons and other degrees of freedom on the chains and in the liquid. A well-known situation occurs when this coupling induces fluctuations of the exciton energy levels on two distinct time scales, very fast (e.g., due to high-frequency exciton–phonon-type interactions) and very slow (e.g., due to long range density fluctuations). This gives rise to homogeneous and inhomogeneous line shapes, respectively. When these two type of system–environment interactions are independent of each other, the absorption line shape of the aggregate is a convolution of the line shapes that result from each individual process.

As discussed in Sec. IV, the perturbations of the aggregate energy levels cause, next to optical dephasing, localization of the electronic excitations. The dynamic character of the coupling with the environment gives rise to time-

dependence of the exciton delocalization length of each aggregate. The delocalization length is therefore directly related to the optical dephasing of an ensemble of excitonic systems. Simply stated, when the dynamic perturbations of the molecular energy levels are small, the delocalization length of the excitons is large, and the optical dephasing is slow.

The delocalization of the excitation has important consequences for the observed broadening of optical transitions, since the exciton averages over many single-molecule fluctuations. This is well-established for static distributions of molecular energies (inhomogeneous broadening), where it was shown that the width of the absorption line shape of an aggregate is narrowed by the square root of the delocalization length ($N^{1/2}$) compared to the distribution in single-molecule energies.[12] This is known as exchange- or motional-narrowing. For very fast fluctuations no such theory exists, but often it is assumed that the homogeneous dephasing rate of excitonic transitions is simply identical to those of the single molecules.[9] This means that the exchange narrowing process is completely ignored for fast single-molecule fluctuations, an assumption that lacks theoretical backing at the moment.

Since exciton dynamics at room temperature is largely determined by phase fluctuations, we decided to perform photon echo experiments on TDBC aggregates in water. In these experiments a short optical pulse with wave vector $\mathbf{k}_1$ creates a coherent superposition of exciton states and the ground state, that subsequently decays due to optical dephasing processes. A second short pulse with wave vector $\mathbf{k}_2$ starts rephasing in the sample when there is memory of the dephasing processes that occurred before. This is for instance the case when the optical dephasing is caused by a static or slowly fluctuating distribution of exciton transition energies. Due to the rephasing, the initial superposition state is then (partly) recovered, which can be observed as a burst of coherent radiation, the photon echo, in the direction $2\mathbf{k}_2$-$\mathbf{k}_1$. When there are additional fluctuations in the sample, with memory times that are short on the time scale of the pulse separation, the photon echo intensity will decrease when the delay between the pulses is increased.[20,21] Thus, the echo signal can be used to separate fast and slow fluctuations of optical transitions, and characterize their time domain behavior.

The layout of the photon echo experiment and results for three different pulse energies are shown in Fig. 6(a). The intensities are rescaled so that the tails of the signals overlap. We find that the shapes of these tails are intensity independent, but that the behavior near zero delay saturates when the pulse energy is increased. It is at the moment not clear what causes this saturation phenomenon. In principle many optical transitions of the aggregate contribute to the observed signals. If we consider the ground state and the $k=1$ one-exciton state as a two-level system, the pulse angle of each optical pulse is in the order of $\Theta \approx \pi/2$.[49] In this limit many other transitions from the ground state to the one-exciton band, from the one-exciton band to the two-exciton band, and probably between higher exciton bands, contribute to the echo signal as well. All these transitions beat against each other, with initial phase factors that are sometimes in-phase and sometimes out of phase with each other. Although photon echo formation under these circumstances has been treated in model calculations by Spano,[50] a quantitative analysis of the high-intensity traces of Fig. 6(a) is very complicated. In addition, it is possible that dynamic Stark shifts of the energy levels also determine the relative phases of the various contributions,[43] which complicates a description even more. We will therefore leave a full account of these effects for a future article.

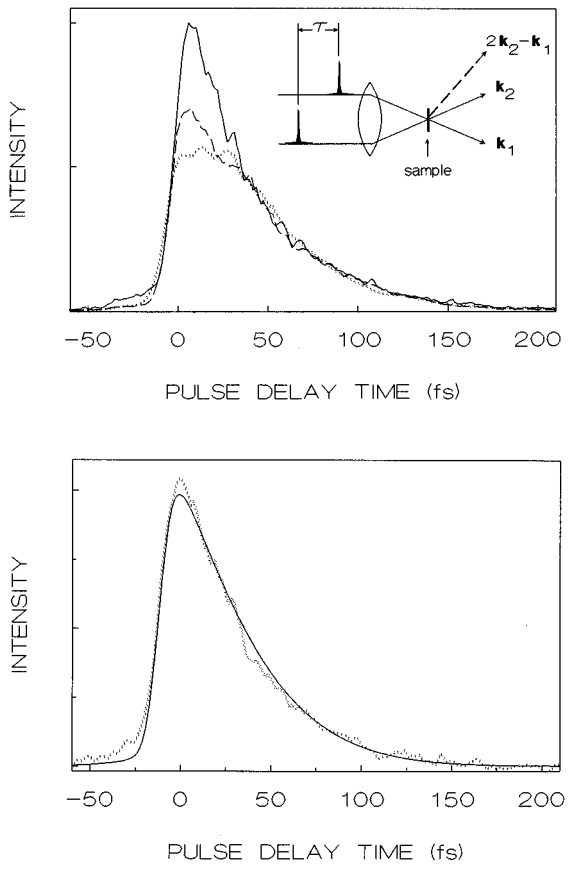

FIG. 6. (a) Two-pulse photon echo decay of TDBC in water for three pulse energies; 0.05 nJ (solid line), 0.15 nJ (dashed line), and 0.25 nJ (dotted line). The layout of the experiment is shown in the inset. The echo intensity increases strongly with pulse energy, but the scales have been readjusted to overlap the tail parts of the decay. Increasing saturation of the signals is evident in the dashed and dotted traces, when the pulse energy becomes higher than ~0.08 nJ. (b) Two-pulse photon echo signal in the low pulse energy, perturbative limit (dotted line). The experimental curve is compared to a theoretical one (solid line), based upon Eq. (21), in which stochastic fluctuations were assumed with correlation times of 5 fs and 10 ps, and amplitudes of 10 THz and 54 THz, respectively.

When the intensity of the optical pulses is lowered, an echo trace is obtained with a shape that does not depend on intensity anymore. Thus, the formation of the echo can be treated in a perturbative way. The contributions from the various transitions are then proportional to the fourth power of the respective oscillator strengths ($\sim\mu_i^8$), with interference terms between them in which powers of each oscillator strength are multiplied. Since the transition from the ground state to the $k=1$ one-exciton state has by far the largest os-

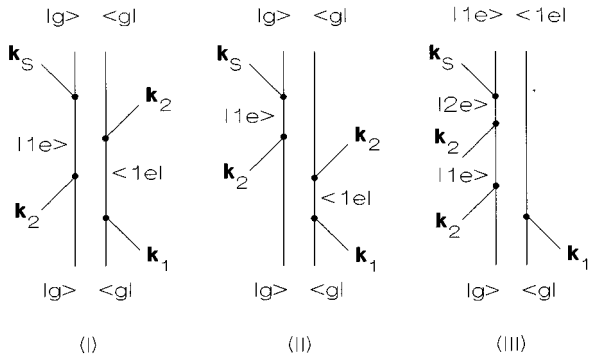

FIG. 7. Double-sided Feynman diagrams for photon echo generation in a three-level system, consisting of a ground state $|g\rangle$, a one-exciton state $|1e\rangle$, and a two-exciton state $|2e\rangle$. The first two diagrams hold for a two-level system as well; the third one, which inherently is out of phase with the first two, is due to the presence of an additional level that can be reached from the first excited state.

cillator strength [Eq. (8)], it dominates the photon echo experiment in these circumstances. To a good approximation contributions from all other transitions from the ground state to the one-exciton band can be ignored. However, this does not mean that the experiment can be treated in a two-level approximation, since transitions from the one- to the two-exciton band have to be considered as well.

The two-exciton band, which can be reached with two system–field interactions, in principle contributes in the perturbative limit to the observed echo trace as well. The strongest transition from the $k=1$ one-exciton state is to the $k_1k_2=2,1$ two-exciton state [Eq. (10)], so the total third order nonlinear response of the aggregates can be described in terms of a three-level system, consisting of a ground state $|g\rangle$, a one-exciton state $|1e\rangle=|k=1\rangle$, and a two-exciton state $|2e\rangle=|k_1=2,\ k_2=1\rangle$. In Fig. 7 is shown that there are three independent contributions to the echo amplitude in such a three-level system. In total there are eight of these diagrams for scattering in the phase matched direction $2\mathbf{k}_2-\mathbf{k}_1$, but only those which contain the possibility of rephasing of optical coherence are represented here. A full account of the echo formation, including the five correction terms without rephasing, will be given elsewhere.[51]

The important point is that there is a contribution, represented by the last diagram of Fig. 7, that is due to the presence of the two-exciton band. This term gives a signal that radiates with the optical frequencies of the one- to two-exciton transitions. Initially, at zero delay, it is out of phase with the two other contributions. This means that destructive interference occurs between the various signal amplitudes.[52] Since the first two terms radiate at the frequency $\omega_{g\rightarrow k=1}$ and the third one at the frequency $\omega_{k=1\rightarrow k1k2=2,1}$, oscillations in the echo intensity occur with the difference frequency $\Delta\omega$, which is given by Eq. (11).

An expression for the echo signal is easily obtained from the diagrams of Fig. 7, when it is assumed that the fluctuations on both optical transitions are correlated. In that case dephasing on one transition can be nullified by rephasing on another one. This correlation was demonstrated some time ago for the inhomogeneous widths of optical transitions in gas-phase[53] and low-temperature solid[54] multilevel systems. For liquids, where there is no proper (static) inhomogeneous width, but rather frequency fluctuations on multiple time scales, this correlation between fluctuations of optical transitions in multilevel systems is not as well established. However, when we assume that the correlation is there, we find that the echo amplitude is proportional to

$$A_{\mathrm{echo}}(t,\tau) \sim \left\{ 2-\frac{\mu_{k_1k_2,k}}{\mu_{k,g}} \times \exp[\,i(\omega_{g\rightarrow k=1}-\omega_{k=1\rightarrow k_1k_2=2,1})(t-\tau)\,] \right\} R_{\mathrm{echo}}(t,\tau). \tag{16}$$

Here, pulse delay τ and time t are counted from the application of the first pulse, and $R_{\mathrm{echo}}(t,\tau)$ is a relaxation function that depends on the dynamical model of the optical system. The first part of Eq. (16) also holds for a two-level system, while the second part is due to the presence of the two-exciton band.

It is usually assumed that at room temperature population relaxation is much slower than optical dephasing, so that its contribution to the line shape of the optical transition(s) can be ignored. However, in case of the multiexciton bands of aggregates this cannot be taken for granted. In the annihilation model of the previous section it was assumed that the lifetime of the two-exciton band is much shorter than any other population relaxation time in the lowest two exciton bands, which gives an upper limit on this lifetime of about $(\gamma_{2e\rightarrow 1e})^{-1}<2$ ps. Now, if we assume that population relaxation is much slower than optical dephasing, a lower limit is obtained as well; $(\gamma_{2e\rightarrow 1e})^{-1}>200$ fs. Since these two limits are compatible, we will ignore population relaxation for the moment in the discussion of optical dephasing.

Instead of assuming the presence of infinitely fast (Markovian) fluctuations, leading to exponential damping processes and Lorentzian line shapes, and infinitely slow (static) fluctuations, leading to inhomogeneous damping processes and line shapes, we will use a more general treatment, and let the aggregate energy levels fluctuate stochastically on two characteristic time scales. This means that the transition frequency of each aggregate varies randomly as $\omega(t)=\omega_0+\delta\omega(t)$. The statistics of the time dependent part, $\delta\omega(t)$, can be evaluated for an ensemble of aggregates in terms of a correlation function that depends on the physics of the system–heat bath interaction.[55,56] For Gaussian statistics of both the fast and slow parts of the fluctuations, this can be written as

$$\langle \delta\omega(t)\,\delta\omega(0)\rangle = \Delta^2_{\mathrm{slow}}\exp(-\Lambda_{\mathrm{slow}}t) + \Delta^2_{\mathrm{fast}}\exp(-\Lambda_{\mathrm{fast}}t). \tag{17}$$

Here, Δ is the root mean square amplitude and Λ is the inverse correlation time $(t_c)^{-1}$ of the excursions of the transition frequencies around the average value ω_0.

Using Eq. (17), all optical relaxation functions can be evaluated. For linear response, the result is[21,28,55,56]

$$R_{\text{linear}}(t)=\exp[-g(t)] \tag{18}$$

while for the echo amplitude of Eq. (16) the relaxation function $R(t,\tau)$ is[21,28,57,58]

$$R_{\text{echo}}(t,\tau)=\exp[-2g(t-\tau)-2g(\tau)+g(t)]. \tag{19}$$

Here, the line shape function $g(t)$ is given by

$$\begin{aligned} g(t)&=g_{\text{slow}}(t)+g_{\text{fast}}(t)\\ &=\frac{\Delta_{\text{slow}}^2}{\Lambda_{\text{slow}}^2}[\exp(-\Lambda_{\text{slow}}t)+\Lambda_{\text{slow}}t-1]\\ &\quad+\frac{\Delta_{\text{fast}}^2}{\Lambda_{\text{fast}}^2}[\exp(-\Lambda_{\text{fast}}t)+\Lambda_{\text{fast}}t-1]. \end{aligned} \tag{20}$$

When the slow fluctuations approach the static limit ($t_c=\Lambda_{\text{slow}}^{-1}\to\infty$), and the fast fluctuations the Markovian limit ($t_c=\Lambda_{\text{fast}}^{-1}\to 0$), the line shape functions are simply $g_{\text{slow}}(t)=\Delta^2t^2/2$ and $g_{\text{fast}}(t)=\Delta^2t/\Lambda$. The relaxation function for linear response Eq. (18) then is the product of a Gaussian and exponential decay, and the corresponding frequency domain spectrum a convolution of a Gaussian and Lorentzian line shape. Thus, conventional inhomogeneous and homogeneous broadening emerge as limits of the more general, non-Markovian treatment adopted here.

In Fig. 6(b) the measured photon echo trace at low pulse energy is compared to a calculation of the signal. Since the detector integrates the echo intensity over all times t, and the optical pulses have a finite duration, the theoretical expression for the signal $S_{\text{echo}}(\tau)$ is

$$S_{\text{echo}}(\tau)=\left\{\int_{\tau}^{\infty}[A_{\text{echo}}(t,\tau)]^2dt\right\}\otimes T(\tau), \tag{21}$$

where $T(\tau)$ is a measure of the time resolution, $\otimes$ designates a convolution, and $R_{\text{echo}}(t,\tau)$ is given by Eq. (16). The theoretical curve of Fig. 6(b) was calculated with Eq. (21), using the line shape function Eq. (20) with parameters values $\Delta_{\text{slow}}=10$ THz, $\Lambda_{\text{slow}}^{-1}=10$ ps and $\Delta_{\text{fast}}=54$ THz, $\Lambda_{\text{fast}}^{-1}=5$ fs. The contribution to the signal from the two-exciton band (the third diagram of Fig. 7) was found to give rise to a decrease of the slope of the echo trace compared to a two-level calculation with the same parameters. This is due to the fact that the two-exciton contribution initially is out of phase with the other terms, causing destructive interference. When the delay time τ is increased, the phase factor develops whereby the destructive interference becomes less efficient.

The echo signals can be fitted with the theory of Eqs. (16)–(21) for a wide range of the four parameters. For instance, the conventional homogeneous/inhomogeneous broadening picture gives a fit as good as the one shown in Fig. 6(b). However, other consequences of the dynamic behavior are not described well in this limit of the optical dynamics. For instance the steady state absorption spectrum, in which fluctuations on all time scales are expressed, is calculated to be much broader than observed experimentally. Vice versa, when the absorption spectrum is fitted as a convolution of homogeneous and inhomogeneous width, the photon echo trace that is calculated is longer than observed experimentally. We therefore have to conclude that the optical dynamics of the TDBC-aggregates in water has to be described in a non-Markovian way, just as was found for single molecules in liquids.[21,22] The absorption spectrum $A(\omega)$ can be calculated by summing over the various transitions from the ground state to the one-exciton band, each broadened by the optical dynamics

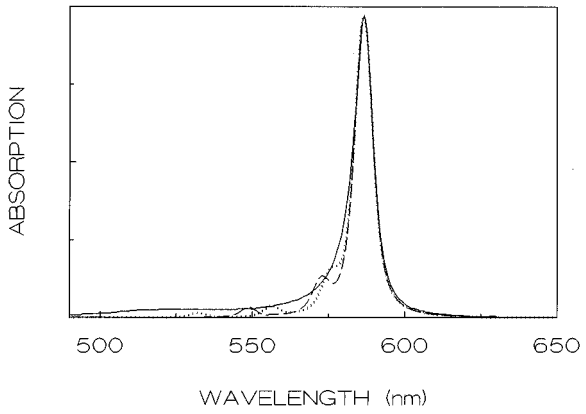

FIG. 8. Absorption spectrum of TDBC in water (solid line), with two calculations based on lineshape function Eq. (22), in which stochastic fluctuations on time scales of 5 fs and 10 ps are assumed, with amplitudes of 10 THz and 54 THz, respectively. The level structure in the one-exciton band shows up as oscillations in the calculated absorption profile, for exciton delocalization lengths of 14 molecules (dashed line) and 16 molecules (dotted line). In the experiment a distribution of delocalization lengths is present, which leads to a smooth asymmetric absorption profile.

$$A(\omega)=\sum_k \omega\mu_{g\to k}^2F(\omega_{g\to k}-\omega), \tag{22}$$

where $F(\omega_{g\to k}-\omega)$ is the real part of the Fourier–Laplace transform of $R_{\text{linear}}(t)$ of Eq. (18),

$$\begin{aligned} F(\omega_{g\to k}-\omega)=2\ \text{Re}\Bigg\{&\int_0^{\infty}dt\ \exp[i(\omega_{g\to k}-\omega)t]\\ &\times R_{\text{linear}}(t)\Bigg\}. \end{aligned} \tag{23}$$

When we use the parameters of the echo trace of Fig. 6(b) to calculate the absorption spectrum with Eq. (22), the experimental trace is simulated rather well. This is shown in Fig. 8, where theoretical absorption spectra are depicted for two aggregates with exciton delocalization lengths $N=14$ and $N=16$. The fluctuations of the delocalization lengths in the sample give rise to the smooth asymmetric absorption profile of the one-exciton band.

The photon echo decays of TDBC aggregates in water, shown in Figs. 6 are longer than ever measured before in a room temperature liquid.[20–26] The reason for this slow optical dephasing is the motional averaging of the exciton over the energetic perturbations, caused by the rapid motions of the molecules in the liquid. Unfortunately, we have no information of the optical dephasing of TDBC monomers to evaluate the averaging process quantitatively. In fact, for water there are no reliable data known to us on the optical dynamics of any single-molecule solution, possibly because

the dynamics is too fast to measure. For the monomer molecules DODCI[25] and HITCI,[26] whose molecular structure is similar to that of TDBC, we found in ethylene–glycol that the parameters of the fast fluctuations are similar to those of TDBC-aggregates in water. The amplitude of the slow fluctuations is considerably less for the aggregates than for the single molecules (about a factor of 6). The correlation times of the slow fluctuations are similar, but this is not a sensitive parameter in the fitting of the echo traces, since the time scale of the experiment is much shorter than this correlation time.

We can conclude from the comparison between the single-molecule data in ethylene–glycol and TDBC-aggregates in water, that motional averaging is effective for the slow components of the fluctuations. The time scale on which the exciton averages over single-molecule properties is much faster than the single-molecule dynamics, so the conventional theory of averaging over static properties holds; the amplitude Δ_{slow} is much smaller for aggregates than for single molecules, and the reduction may well be described by the static $N^{1/2}$ scaling law, mentioned at the beginning of this section.[12]

The situation for the fast part of the fluctuations is less clear. The parameters Δ_{fast} and Λ_{fast} that we find for TDBC-aggregates in water, are similar to those of DODCI and HITCI single-molecules in ethylene glycol. This would seem to indicate that motional averaging has no effect on these fluctuations. On the other hand, it can be expected that the fluctuations are faster and have larger amplitudes in water than in ethylene glycol. Then the similarity of the parameters is accidental, and motional averaging *does* affect the fast part of the fluctuations. The efficiency of motional averaging on fast fluctuations is determined by time scales. When the single-molecule fluctuations are infinitely fast (compared to the exciton averaging motion), each fluctuation event is an independent process. In this limit no motional averaging can be expected. When the single-molecule fluctuations occur over a certain time-span, characterized by a finite correlation time $\Lambda_{\text{fast}}^{-1}$, motional averaging can take place, with an efficiency determined by the time scale of the coherent exciton motion. A microscopic theory for this general case has not yet been formulated.

VII. CONCLUSIONS

The population decay and optical dephasing of room temperature molecular aggregates were studied by pump–probe experiments, grating scattering, fluorescence life time experiments and two-pulse photon echoes. In all of these experiments it turned out to be insufficient to look at the one-exciton band only. From the grating scattering and photon counting experiments it was concluded that the two-exciton band participated in the population kinetics of the excitons, by serving as a decay channel for the one-exciton band through exciton–exciton annihilation. The transitions from the one-exciton band to the two-exciton band were employed in frequency-resolved pump–probe experiments to establish the average delocalization length of the excitons along the aggregate chains. And finally, it was found that the two-exciton band could not be ignored in the photon echo experiments either, not even when the pulse intensities were lowered to the perturbative limit of system–field interaction.

No evidence was found in any of our data for states that are split-off from the main multiexciton bands, such as for example biexcitons from the two-exciton band. Such states would arise from specific physical interactions between excitons on the same chain. Whereas the presence of multiexciton bands cannot be ignored in nonlinear optical experiments with broad bandwidth pulses, the same holds for states in which two or more excitons interact. Yet, for instance in the frequency-resolved pump–probe data, no additional excited state resonances outside of the two-exciton band were observed. This substantiates our approach to the aggregate dynamics, in which interexcitonic interactions were completely ignored.

The various aspects of the optical dynamics are all related through the influence of the dynamic perturbations on the aggregates in the liquid. These perturbations determine the optical dephasing of the electronic transitions of the aggregates, influence the diffusion of the excitons along the chains and thereby the exciton–exciton annihilation process, and determine the delocalization length of the excitons. These parameters, that were all studied experimentally, are therefore directly related. The results of the different experiments were discussed in terms of a single model, based on homogeneous aggregates with nearest-neighbor coupling and phenomenological damping parameters. The conclusions on the delocalization length, population relaxation pathways, and optical dephasing of TDBC-aggregates in water are to some extent general, and do not depend on the specific model. The parameter values may be affected, though, when more detailed microscopic descriptions will be used.

The effect of motional narrowing on fast and slow fluctuations was discussed. The narrowing of the exciton absorption spectrum compared to the monomer spectrum was shown to be mainly due to a reduction of the slow fluctuations (inhomogeneous broadening). For these slow fluctuations the conventional theory of static disorder may well apply, while for fast fluctuations the situation is still very complex. The interpretation of the experimental results will eventually have to be performed in a microscopic description, that directly links the dynamic behavior of the single molecules to that of the excitons. New experimental data on the complex electronic structure and dynamics of aggregates will be of utmost importance to construct a reliable theory in this respect.

ACKNOWLEDGMENTS

We would like to thank J. Moll for pointing out TDBC aggregates to us, and J. Knoester for discussions on multiexciton bands. The investigations were supported by the Netherlands Foundation for Chemical Research (SON) and Physical Research (FOM) with financial aid from the Netherlands Organization for the Advancement of Science (NWO).

[1] A. H. Herz, Adv. Colloid Interface Sci. **8**, 237 (1977).
[2] V. Sundström and R. van Grondelle, J. Opt. Soc. Am. B **7**, 1595 (1990).
[3] G. Scheibe, Z. Elektrochem. **52**, 283 (1948).
[4] Y. Wang, J. Opt. Soc. Am. B **8**, 981 (1991).

[5] V. L. Bogdanov, E. N. Viktorova, S. V. Kulya, and A. S. Spiro, JETP Lett. **53**, 105 (1991).
[6] S. de Boer, K. J. Vink, and D. A. Wiersma, Chem. Phys. Lett. **137**, 99 (1987).
[7] P. O. J. Scherer and S. F. Fischer, Chem. Phys. **86**, 269 (1984).
[8] E. Hanamura, Phys. Rev. B **37**, 1273 (1988).
[9] F. C. Spano and S. Mukamel, Phys. Rev. A **40**, 5783 (1989).
[10] P. W. Anderson, Phys. Rev. **109**, 1492 (1958).
[11] M. Schreiber and Y. Toyozawa, J. Phys. Soc. Jpn. **51**, 1528 (1981).
[12] E. W. Knapp, Chem. Phys. **85**, 73 (1984).
[13] F. C. Spano and S. Mukamel, J. Chem. Phys. **91**, 683 (1989).
[14] A. Boukahil and D. L. Huber, J. Lumin. **45**, 13 (1990).
[15] H. Fidder, J. Knoester, and D. A. Wiersma, J. Chem. Phys. **95**, 7880 (1991).
[16] A. Tilgner, H. P. Trommsdorff, J. M. Zeigler, and R. M. Hochstrasser, J. Chem. Phys. **96**, 781 (1992).
[17] J. Knoester, Chem. Phys. Lett. **203**, 371 (1993).
[18] J. R. Durrant, J. Knoester, and D. A. Wiersma, Chem. Phys. Lett. **222**, 450 (1994).
[19] C. H. Brito-Cruz, R. L. Fork, W. H. Knox, and C. V. Shank, Chem. Phys. Lett. **132**, 341 (1986).
[20] P. C. Becker, H. L. Fragnito, J.-Y. Bigot, C. H. Brito-Cruz, R. L. Fork, and C. V. Shank, Phys. Rev. Lett. **63**, 505 (1989).
[21] E. T. J. Nibbering, D. A. Wiersma, and K. Duppen, Phys. Rev. Lett. **66**, 2464 (1991).
[22] J.-Y. Bigot, M. T. Portella, R. W. Schoenlein, C. J. Bardeen, A. Migus, and C. V. Shank, Phys. Rev. Lett. **66**, 1138 (1991).
[23] D. A. Wiersma, E. T. J. Nibbering, and K. Duppen, Springer Ser. Chem. Phys. **55**, 611 (1993).
[24] T. Joo and A. C. Albrecht, Chem. Phys. **176**, 233 (1993).
[25] E. T. J. Nibbering, D. A. Wiersma, and K. Duppen, Chem. Phys. **183**, 167 (1994).
[26] W. de Boeij, M. S. Pshenichnikov, K. Duppen, and D. A. Wiersma, Chem. Phys. Lett. **224**, 243 (1994).
[27] E. T. J. Nibbering, D. A. Wiersma, and K. Duppen, Phys. Rev. Lett. **68**, 514 (1992).
[28] K. Duppen, F. de Haan, E. T. J. Nibbering, and D. A. Wiersma, Phys. Rev. A **47**, 5120 (1993).
[29] E. T. J. Nibbering, K. Duppen, and D. A. Wiersma, J. Photochem. Photobio. A Chem. **62**, 347 (1992).
[30] S. Makio, N. Kanamaru, and J. Tanaka, Bull. Chem. Soc. Jpn. **53**, 3120 (1980).
[31] M. Lindrum, A. Glismann, J. Moll, and S. Daehne, Chem. Phys. **178**, 423 (1993).
[32] A. S. Davydov, *Theory of Molecular Excitons* (Plenum, New York, 1971).
[33] D. B. Chesnut and A. Suna, J. Chem. Phys. **39**, 146 (1963).
[34] F. C. Spano, Phys. Rev. Lett. **67**, 3424 (1991); **68**, 2976 (1992).
[35] J. Knoester, Phys. Rev. A **47**, 2083 (1993).
[36] M. Kasha, H. R. Rawls, and M. Ashraf El-Bayoumi, Pure Appl. Chem. **11**, 371 (1965).
[37] J. Moll, S. Daehne, J. R. Durrant, and D. A. Wiersma (submitted).
[38] F. C. Spano, V. Agranovich, and S. Mukamel, J. Chem. Phys. **95**, 1400 (1991).
[39] H. Fidder, J. Knoester, and D. A. Wiersma, J. Chem. Phys. **98**, 6564 (1993).
[40] K. Minoshima, M. Taiji, K. Misawa, and T. Kobayashi, Chem. Phys. Lett. **218**, 67 (1994).
[41] A. E. Johnson, S. Kumazaki, and K. Yoshihara, Chem. Phys. Lett. **211**, 511 (1993).
[42] F. C. Spano, Chem. Phys. Lett. **220**, 365 (1994).
[43] R. Gagel, R. Gadonas, and A. Laubereau, Chem. Phys. Lett. **217**, 228 (1994).
[44] D. V. Brumbaugh, A. A. Muenter, W. Knox, G. Mourou, and B. Wittmershaus, J. Lumin. **31-32**, 783 (1984).
[45] H. Stiel, S. Daehne, and K. Teuchner, J. Lumin. **39**, 351 (1988).
[46] V. Sundström, T. Gillbro, R. A. Gadonas, and A. Piskarskas, J. Chem. Phys. **89**, 2754 (1988).
[47] M. D. Fayer, Annu. Rev. Phys. Chem. **33**, 63 (1982).
[48] D. A. Wiersma and K. Duppen, Sci. **237**, 1147 (1987).
[49] If we take the exciton delocalization length as 15 molecules, the transition dipole $\mu_{k=1,g}$ is 24 D. With 10 fs pulses of 0.2 nJ this gives $\Theta \approx \pi/2$.
[50] F. C. Spano, J. Phys. Chem. **96**, 2843 (1992).
[51] M. van Burgel, D. A. Wiersma, and K. Duppen (to be published).
[52] J. L. Skinner, H. C. Anderson, and M. D. Fayer, J. Chem. Phys. **75**, 3195 (1981).
[53] T. W. Mossberg, A. M. Flusberg, R. Kachru, and S. R. Hartmann, Phys. Rev. Lett. **42**, 1665 (1979).
[54] K. Duppen, D. P. Weitekamp, and D. A. Wiersma, Chem. Phys. Lett. **108**, 551 (1984).
[55] R. Kubo, in *Fluctuations, Relaxation and Resonance in Magnetic Systems*, edited by D. ter Haar (Oliver and Boyd, Edinburgh, 1962), p. 23.
[56] J. R. Klauder and P. W. Anderson, Phys. Rev. **125**, 912 (1962).
[57] B. D. Fainberg, Opt. Spectrosc. (USSR) **55**, 669 (1983).
[58] R. F. Loring and S. Mukamel, Chem. Phys. Lett. **114**, 426 (1985).